Hindawi
International Journal of RF and Microwave Computer-Aided Engineering
Volume 2023, Article ID 2405200, 11 pages
https://doi.org/10.1155/2023/2405200

Research Article

A High Gain Vivaldi Antenna with Multiple Near-Field Dielectric Lenses and Grooved Edges

Manlai Ding,[1] **Xuemei Wang**,[1] **YinShen Wang**,[1] **Zhiwei Hu**,[2] **Gang Liu**,[2] **Ziyan Liu**,[2] **and Bingnan Wang**[1]

[1]*Aerospace Information Research Institute, China Academy of Science, Beijing, China*
[2]*School of Microelectronics, Hefei University of Technology, China*

Correspondence should be addressed to Xuemei Wang; wangxm521@163.com

Received 11 January 2023; Revised 30 April 2023; Accepted 11 May 2023; Published 31 May 2023

Academic Editor: Merih Palandoken

In order to expand the applications of the traditional Vivaldi antenna by addressing the low gain of the traditional Vivaldi antenna, this paper combines the phase distribution of the Vivaldi antenna aperture based on the analysis of the transmission characteristics of a dielectric unit by utilizing the advantages of artificial electromagnetic material. A more reasonable method of loading a dielectric lens is proposed and utilized in combination with edge grooving. A comparison of the results shows that the antenna operates in the frequency range of 4 to 16 GHz. The low-frequency boost is approximately 3 dB, and the high-frequency boost is approximately 9.6 dB.

1. Introduction

Because of the good end-fire characteristics of Vivaldi antennas, these antennas are widely used in imaging systems [1], ultrawideband arrays, ground-penetrating radar systems, etc. [2]. Vivaldi antennas have numerous advantages, such as an ultrawide operating band, a low-profile structure, high gain, and good compatibility in planar printed circuits. Many researchers showed interest in such an antenna when Gibson designed the first Vivaldi antenna in 1979. There have been exciting research results on the improvement of this type of tapered slot antenna (TSA) in different applied scenarios. Vivaldi antennas are generally divided into antipodal [3] and balanced antipodal structures [4]. The former structure is easy to feed, and the latter has lower cross-polarization.

Although a large number of research results on TSA have been published, Vivaldi antennas remain a challenging research topic in regard to miniaturized design, improvement of radiation characteristics, extension of the impedance, and gain bandwidth. In particular, the improvement of the gain and directionality of the Vivaldi antenna has been a major research hotspot. In addition to the antenna array, the high-gain single antenna has great potential for application because it has many advantages, such as its small size, simple structure, convenient design, and low cost. It is currently used in imaging systems [5]. The corrugation edge technique is a common improvement method for the low-frequency performance of Vivaldi antenna, which can provide a rectangular slot edge, a tapered slot edge [6], an exponential slot edge [7], triangular-shaped slits [8], and so on. Unfortunately, this technology offers a limited increase in the gain of the high-frequency band and even produces a certain degree of deterioration. With the rise of metamaterial research, the radiation characteristics of TSA's artificial material have been investigated [9]. A compact structure and higher gain of the antenna can be obtained by embedding the IA-ZIM metamaterial unit into the conventional Vivaldi antenna (CVA) [10]. However, the IA-ZIM metamaterial composed of resonant meander-line unit cells has a narrow working bandwidth. A broadband metamaterial composed of nonresonant parallel-line unit cells was designed in [11]. The metamaterial served for enhancing the gain of a conventional antipodal Vivaldi antenna (CAVA) [12]. Recently, the influence of the layout of the metamaterial unit on the antenna's gain has been studied [13], which further

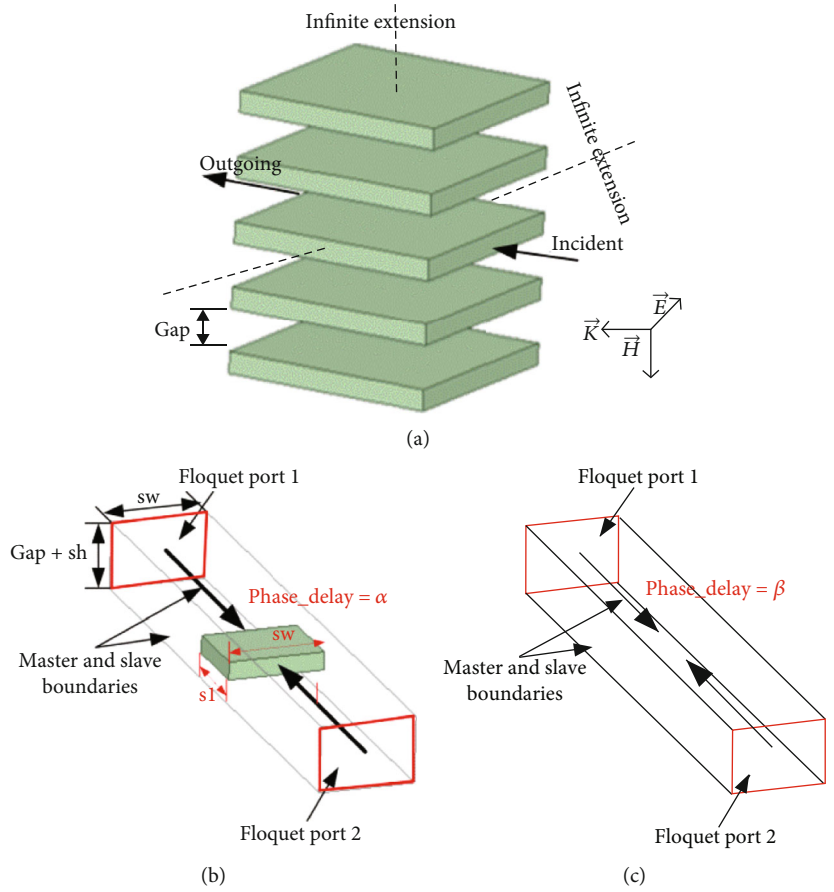

FIGURE 1: (a) Configuration of the infinite periodic substrate of dielectric and (b, c) simulated model in HFSS.

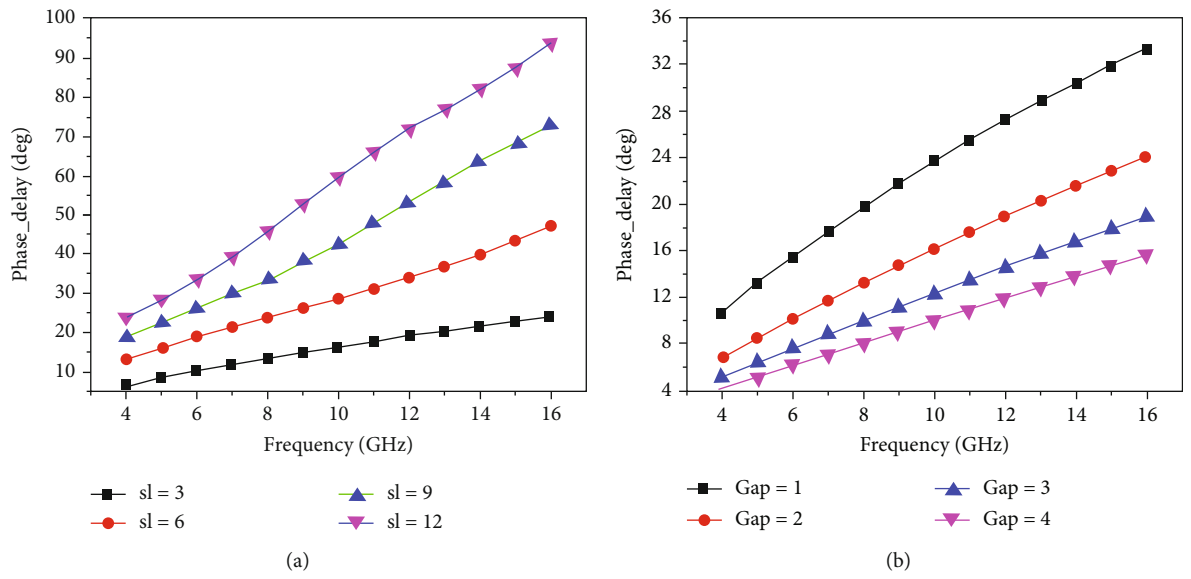

FIGURE 2: (a, b) Phase delay characteristic (α-β) of the RF-45 dielectric unit cell when the length sl and the arrangement spacing gap.

developed the advantages of loading artificial material units. The phase difference of the Vivaldi antenna's aperture was analyzed in [14], which considered the metamaterial loading to compensate for the phase error. The layout of the unit is determined to reduce the phase difference of the aperture and improve the gain of the antenna. However, designing metamaterial processes is cumbersome, the working bandwidth of the unit is limited, and insertion loss will be

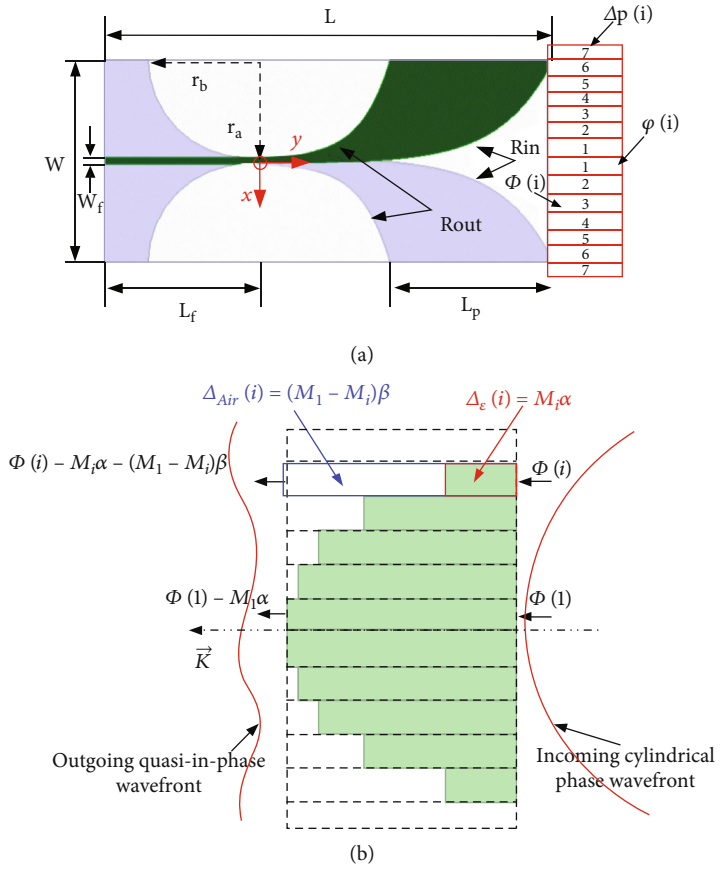

FIGURE 3: (a, b) Mechanism underlying the lens' design.

introduced. The gain of the antenna at high frequencies can be significantly improved by loading the dielectric director and the dielectric lens in the front end of the antenna aperture. For example, that article has improved the radiation characteristics of the antenna by inserting a dielectric rod [15] into the CAVA. Many researchers are interested in enhancing the radiation characteristics of the antenna by adding a dielectric lens in front of the antenna aperture [16]. A simple technique of substrate end shaping was presented in a previous article [17], which corrects the tilted bean and low axial gains of the antenna in the upper working frequencies. A method that significantly improved the antenna gain in high frequencies by applying an elliptical dielectric lens in front of the balanced antipodal Vivaldi antenna's aperture was proposed in [18], but this approach greatly increased the antenna's profile. Recently, several methods for designing dielectric lenses have been proposed. The paper proposes a method of loading a dielectric lens at the focal point to coincide with the intersection of two tangent lines [19]. The author viewed the antipodal Vivaldi antenna as an ideal point source antenna at the focal point and designed the outer-edge shape of the dielectric lens based on Fermat's principle. In another article, the antipodal Vivaldi antenna (AVA) loaded with a dielectric lens of a higher dielectric constant with a shape that follows an exponential structure in its inner and outer edges is proposed [20]. The gain of the antenna was improved, and a 3 dB beam width is reduced by approximately 24%. In the following article [21], the proposed antenna provides a 7.5 dB improvement in antenna gain in high frequencies by adding a trapezoid-shaped dielectric lens in front of the AVA.

TABLE 1: Design parameters of the antenna (unit: mm).

R_{out}	R_{in}	L_f	L_p	W_f	W	L	r_a	r_b
0.14	0.08	35	40	1.45	50	110	25	35

A new method of applying a near-field dielectric lens in front of the CVA is proposed in this paper, which can significantly improve the radiation performance in the ultrawideband frequency range. The position of the focal point of the dielectric lens is not easy to determine because the phase center of the CVA obviously changes with the operating frequency, which introduces theoretical difficulties in the lens design. Therefore, in this paper, the outer-edge shape of the lens is designed by correcting the near-field phase error at the CVA aperture. First, the E-filed phase distribution should be extracted at the antenna's aperture. The phase delay characteristics of the dielectric unit clearly are analyzed in the second part of the article, and the basic theory of compensation is provided for the design of a broadband near-field dielectric lens. In the third part of the paper, the designing process of the AVA-loaded near-field dielectric lens is introduced, and its radiation performance is analyzed.

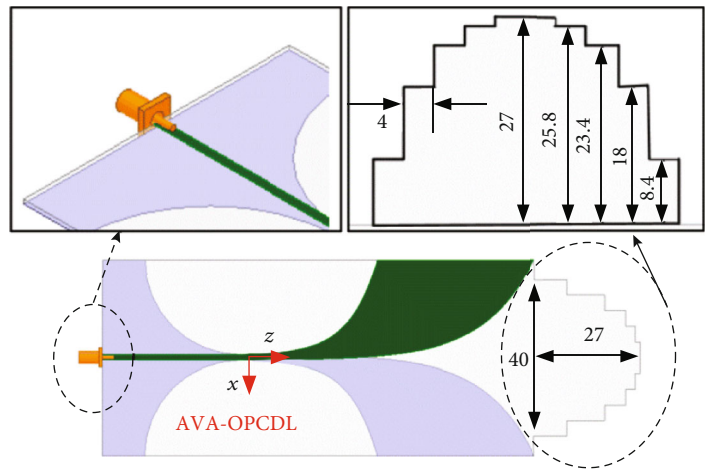

Figure 4: Structure of the AVA-OPCDL.

Table 2: Detailed design parameters of the dielectric lens.

x	Phase	Delta	Relative delta	Number of units
2	-18	0	144	9
6	-24	6	138	8.6
10	-38	20	124	7.8
14	-66	48	96	6
18	-118	100	44	2.8
22	-162	144	0	0

In the fourth part of this paper, the proposed antenna is analyzed by the measured and simulation results, and the performance of the fabricated antenna is summarized. Finally, the conclusion and outlook are provided in the fifth part of this paper.

2. The Method of Loading Dielectric Lens

As shown in Figure 1(a), the phase of electromagnetic waves will be delayed when traversing through an infinite periodic substrate of a dielectric. The simulated models are illustrated in Figures 1(b) and 1(c). The boundaries are assigned as a periodic boundary. The Floquet ports are placed at a distance of 10 mm from the closest face of the dielectric unit, and the phase of the transmitted EM wave is computed at the surface of the dielectric unit, as shown in Figure 1.

The material of the unit is selected as Taconic RF-45 (with a relative permittivity of 4.5) and air; the phase delay shifts are, respectively, set to α and β. The characteristic of the phase delay (α-β) of the RF-45 dielectric unit is shown in Figure 2(a). The result shows that the phase delay increases with the increase in frequency when the dielectric unit length is fixed, and a certain linear relationship can be observed. Let δ_f be the amount of phase delay at 10 GHz when the length is constant. Then, the phase delay of each frequency can be calculated by $p_f = f/10 \times \delta_f + c$ and c is the fitting error constant, which is controlled within 5°. Moreover, the phase delay will be considerably changed by controlling the length of the dielectric unit. By referring to

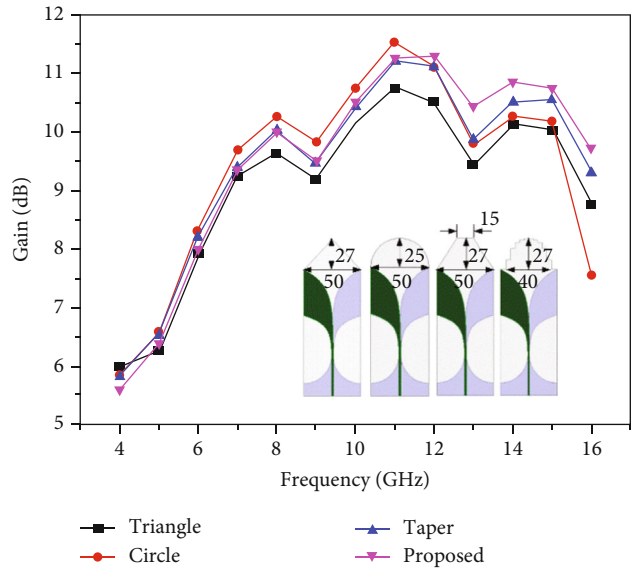

Figure 5: Comparison of antenna gain after loading with differently shaped lenses.

Figure 2(a), it can be seen that the length of the unit is approximately proportional to the phase delay. At the same frequency, the $p_l = l \times \delta_l + c$ can be used to calculate the total phase delay of the unit. In the above formula, p_l represents the total phase delay shifts of length l, δ_l represents the phase delay characteristic of each length, c is the fitting error. The value of c is controlled between 1° and 6°, which can be neglected from the analysis of multiple sets of experimental data. The influence of the periodic arrangement spacing of the unit on the phase delay characteristics is illustrated in Figure 2(b). The results show that the phase delay of the unit decreases with an increase in the gap.

3. Design and Discussion of Vivaldi Antenna of Wideband Near-Field Dielectric Lens

3.1. Design of Prototype Antenna and Broadband Near-Field Dielectric Lenses. According to the article [19] and as shown

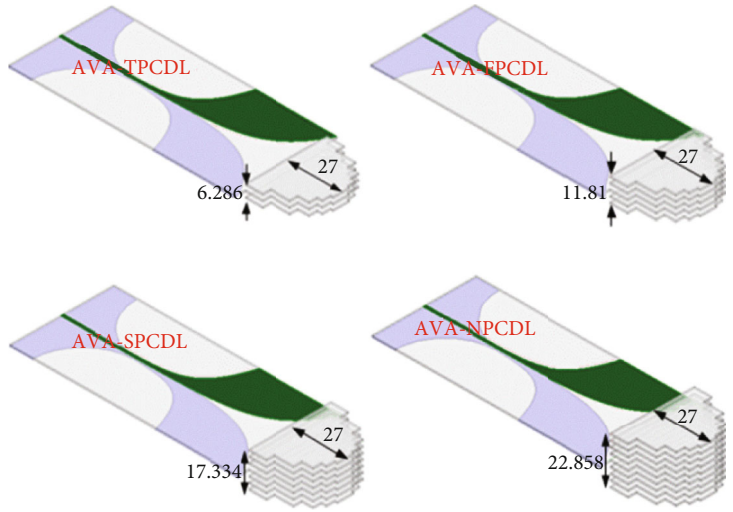

Figure 6: Structure of the AVA loaded with three-layer PCDL, five-layer PCDL, seven-layer PCDL, and nine-layer PCDL.

in Figure 3, a prototype of the CAVA is designed. The prototype is printed on the Taconic RF-45 substrate (relative permittivity of 4.5, a loss tangent of 0.0037) and a thickness of 0.79 mm. The overall size is $50 \times 110 \times 0.79\,\text{mm}^3$. The inner and outer edges of the radiation flares fit the following exponential curves: C_1 and C_2 are determined by the following equations:

$$y = C_1 e^{\text{Rx}} + C_2, \tag{1}$$

$$C_1 = \frac{y_1 - y_2}{e^{\text{Rx}_2} - e^{\text{Rx}_1}}, \tag{2}$$

$$C_2 = \frac{y_2 e^{\text{Rx}_2} - y_1 e^{\text{Rx}_1}}{e^{\text{Rx}_2} - e^{\text{Rx}_1}}, \tag{3}$$

where (x_1, y_1) and (x_2, y_2) are the starting point and ending point of the curve, which can be calculated from the size of the antenna, R is the opening rate of the exponential curve, which has a significant effect on the radiation characteristics of the antenna, R_{in} is set to 0.08 by the opening rate of the inner curve, and R_{out} is set to 0.14 by the opening rate of the outer curve. The balun is elliptical, and the center of the elliptical is (25, 0). The long axis radius is r_b, and the short axis radius is r_a. The size of the antenna parameters is shown in Table 1.

Designing the shape of the lens is based on the analysis of the phase error of the CAVA aperture. In Figure 3(a), the antenna aperture surface is discretized in the x-direction, and the electric field phases are statistically analyzed at $x = 2$ mm, 6 mm, 10 mm, 14 mm, 18 mm, and 22 mm, corresponding to areas 1 to 6. The width of each area is 4 mm, which is equal to the width of the dielectric unit. In this paper, the antenna works at 10 GHz that is assigned as the designed point. Different numbers of the units are, respectively, placed in zones 1 to 6 under the phase error of the antenna's aperture at 10 GHz. M_i is assumed to be the number of dielectric units placed in each area. The $\Delta_\varepsilon(i) = M_i\alpha$ represents the phase

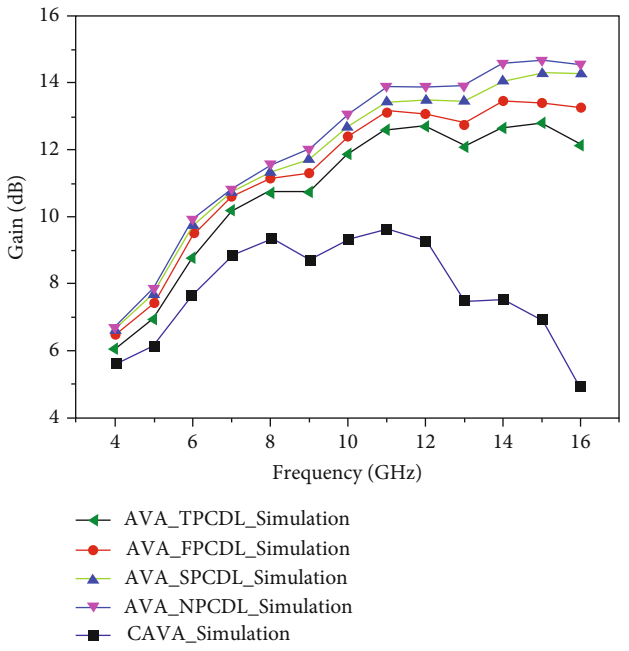

Figure 7: Variation of end-fire gain when different antenna loading layers are used in near-field dielectric lenses.

delay produced by electromagnetic wave passing through the dielectric. $\Delta_{\text{Air}}(i) = (M_1 - M_i)\beta$ denotes the phase delay generated by an electromagnetic wave passing through the air. $\Delta_p(i) = \Delta_\varepsilon(i) + \Delta_{\text{Air}}(i)$ is the total phase delay shifts. Assuming that the phase is $\varphi(i)$ and that we want to achieve the same value at the end of each region, the following formula can be obtained: $\varphi(i) = \Phi(i) - \Delta p(i) = \Phi(i) - \Delta_\varepsilon(i) - \Delta_{\text{Air}}(i)$. The number of dielectric units in each area is determined by using the following formula:

$$\Phi(1) - \Phi(i) = M_1\alpha - M_i\alpha - (M_1 - M_i). \tag{4}$$

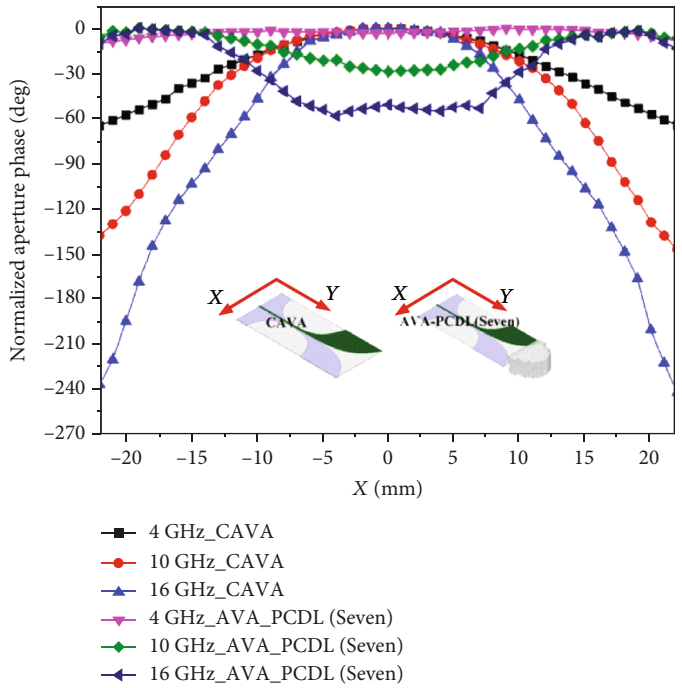

Figure 8: Normalized aperture phase distribution along x direction at 4 GHz/10 GHz/16 GHz for CAVA and AVA-SPCDL.

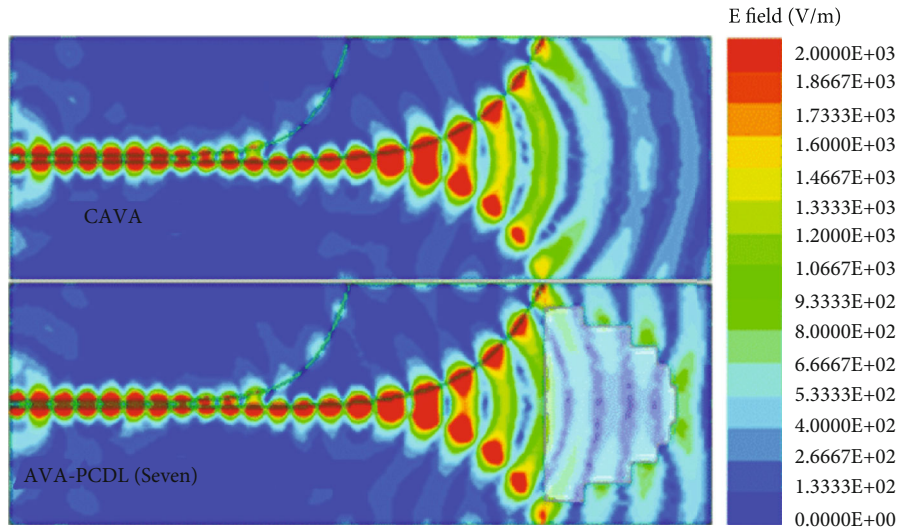

Figure 9: Electric field distribution of the traditional antipodal and the antipodal Vivaldi antenna loaded with dielectric lens.

The derivation is as follows:

$$M_i = M_1 - \frac{\Phi(1) - \Phi(i)}{\alpha - \beta}. \tag{5}$$

The overall size of the lens is $40 \times 27 \times 0.79\,\text{mm}^3$. The lens is designed in a way that converts the incident near-spherical or cylindrical wave into an emergent near-plane wave, as shown in Figure 3(b). The shape of the dielectric lens is shown in Figure 4. The outer edge of the proposed lens is symmetrically serrated. The final lens design parameters are provided in Table 2.

3.2. The Design Process and Final Structure of the Antenna. The single-layer lens is designed on the front of the CAVA, as shown in Figure 4. The overall size of the antenna when loaded with the one-layer lens is $50 \times 137 \times 0.79\ \text{mm}^3$.

Figure 5 shows the end-fire gain curve of the CAVA loaded with different shapes of dielectric lenses. At high frequencies, the shape of the lens has the best gain enhancement effect relative to other settings described in this paper. Compared to the CAVA loaded with a semicircular

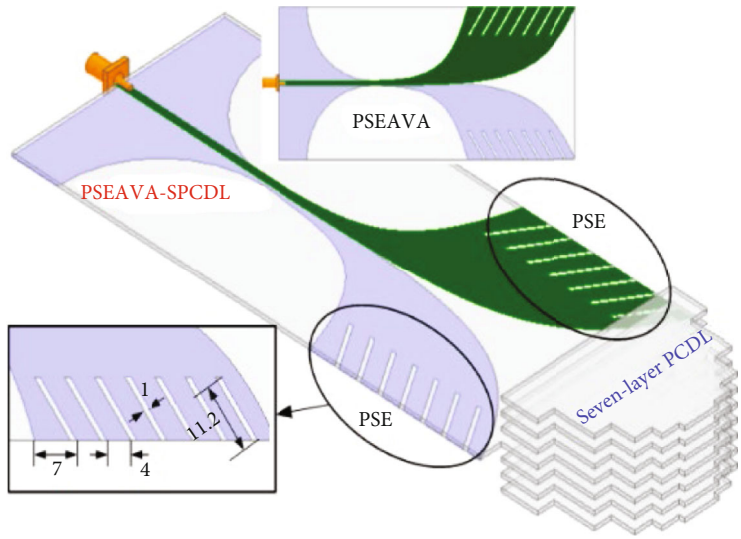

Figure 10: Structure of final design combining seven-layer PCDL and PSE.

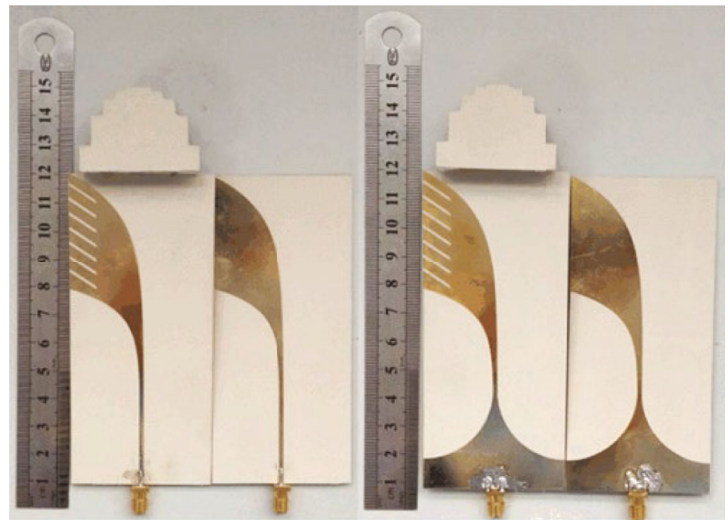

Figure 11: The photograph of the fabricated antennas with SMA connector.

dielectric lens, the gain of the AVA-OPCDL increases by approximately 2.1 dB at 16 GHz. The AVA with three-layer PCDL, five-layer PCDL, seven-layer PCDL, and nine-layer PCDL are designed in order to show the influence of loading multilayer lenses upon the antenna gain. The dimensions of each antenna are marked as shown in Figure 6, and the simulation gain curve is shown in Figure 7.

As shown in Figure 7, the antenna's gain is also improved with the increase in the number of lens layers. It can be seen that the end-fire gain of the antipodal Vivaldi antenna loaded with the seven-layer lens (AVA-SPCDL) and the nine-layer lens (AVA-NPCDL) has approximately the same value. To make the antenna size smaller and more compact, the number of layers of the lens is set to seven layers. The antenna's end-fired gain improves from 4.9 dB to 14.3 dB at the operating frequency of 16 GHz. The gain ranges from 1 to 9.4 dB within the operating frequency band of 4-16 GHz. To illustrate the principle that a broadband near-field dielectric lens enhances the antenna's gain, we experimentally studied the CAVA and AVA antennas with the described loaded dielectric lenses. As shown in Figure 8, the normalized phase difference distribution of the antenna's aperture surface is shown in the x horizontal direction. The phase distribution of the AVA-SPCDL's aperture is approximately flat. However, the phase distribution of the center and the edge of the aperture is still slightly different. The uniform trend is even more obvious with the frequency increase because the periodic conditions of the dielectric unit at the edge are truncated. The characteristics of the phase delay of the medium will be weakened to some extent. Therefore, the phase of the center of the AVA-SPCDL's aperture will have a similar phenomenon of overcompensation. In addition, it can be seen that the effect of this truncation is more pronounced at high frequencies.

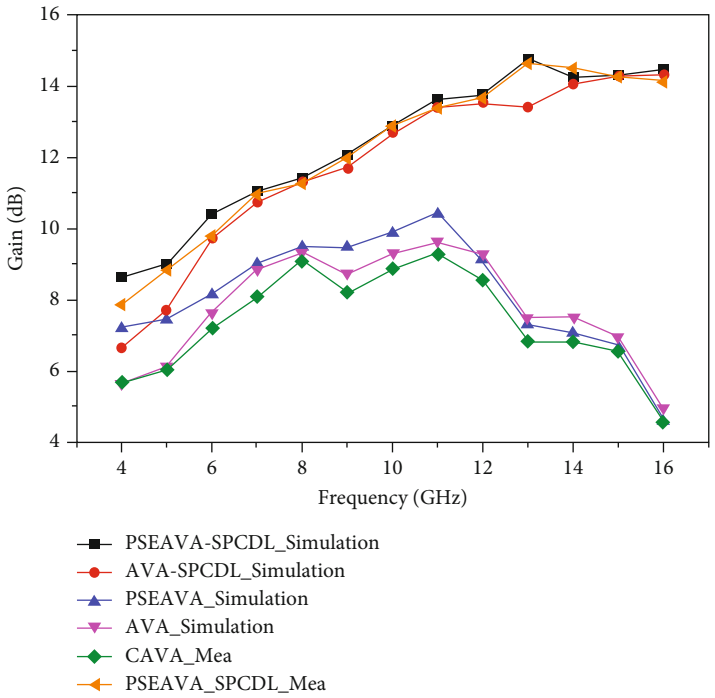

FIGURE 12: Simulated and measured results and the reflection coefficient of the PSEAVA-SPCDL from 4 to 16 GHz.

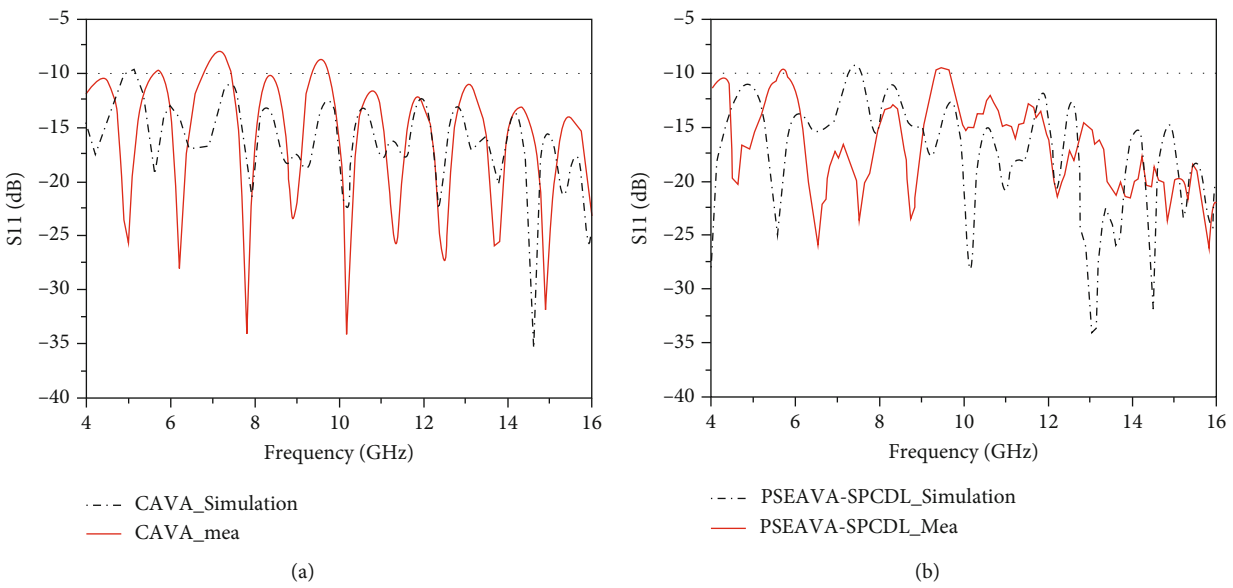

FIGURE 13: Simulated and measured results of (a) the reflection coefficient and (b) the gain of the CAVA and PSEAVA-SPCDL from 4 to 16 GHz.

Figure 9 presents the electric field distribution of the CAVA and the AVA-SPCDL at 16 GHz in the *xy*-plane. The AVA-SPCDL antenna has a flatter electromagnetic wavefront, and its electric field intensity is significantly larger than that of the CAVA antenna at the center of the aperture. From the above analysis, the proposed dielectric lens contributes to phase compensation and guiding convergence for the electromagnetic waves of the CAVA antenna's aperture.

When combined, the antenna's end-fire gain performance is significantly better than that of the previous articles because the antenna is loaded with a lens that has a relatively low gain in the low-frequency band. The slit edge technique is applied in order to improve the gain at lower frequencies, thus creating a periodic slit edge AVA-SPCDL (PSEAVA-SPCDL). The structure of PSEAVA-SPCDL is shown in Figure 10. The initial design of slits is set according to the

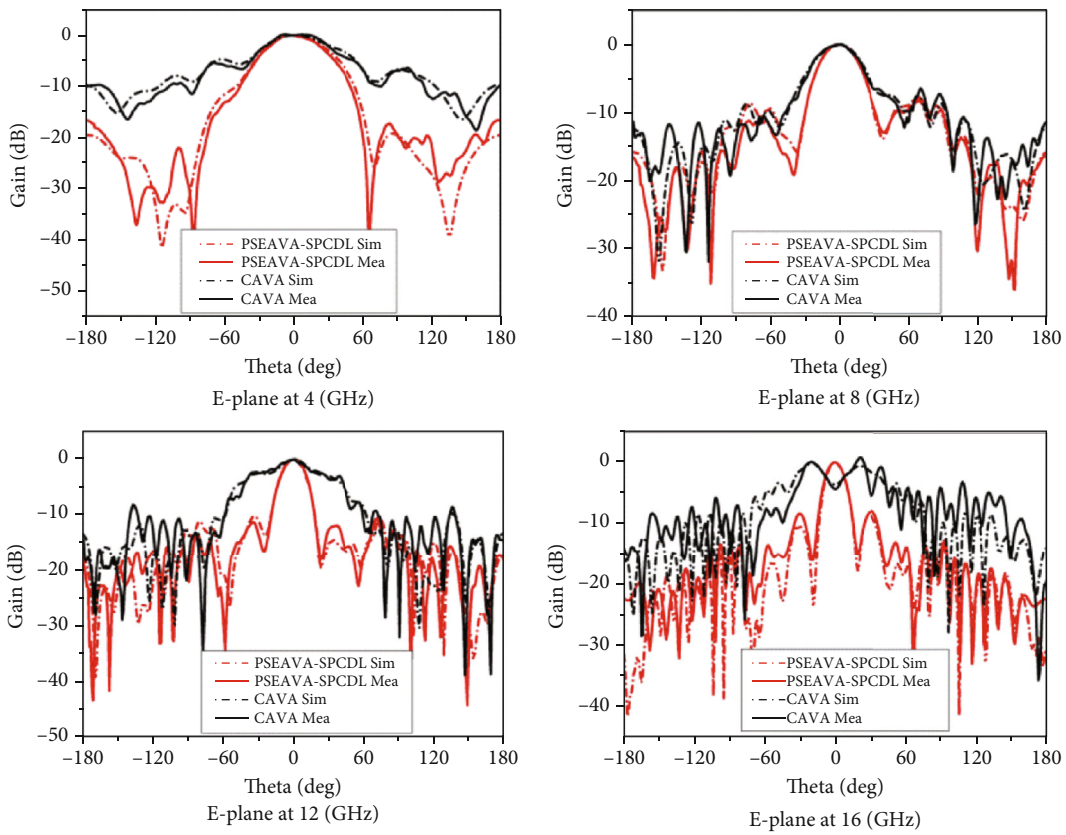

Figure 14: The *E*-plane radiation patterns of the CAVA and PSEAVA-PCDL at 4 GHz/8 GHz/12 GHz and 16 GHz.

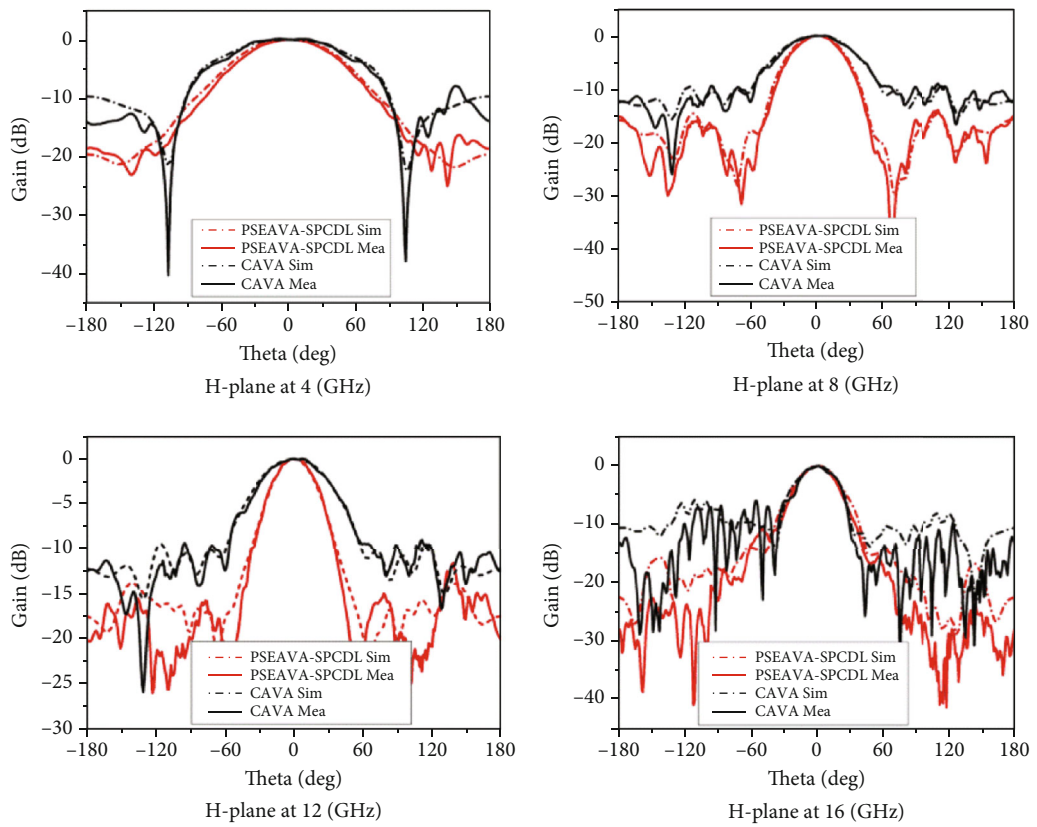

Figure 15: The *H*-plane radiation patterns of the CAVA and PSEAVA-PCDL at 4, 8, 12, and 16 GHz.

Table 3: Comparison between the proposed antenna and literature.

Ref	Dimensions (mm)	Bandwidth (GHz)	Gain (dB)	Sidelobe (dB)
[20]	$76 \times 130 \times 1$	3.1-14	1.2-8.3	11
[2]	$96 \times 140 \times 0.508$	1-30	2.2-11	—
[6]	$40 \times 90 \times 0.508$	3-40	8-14	10
[22]	$30 \times 55 \times 0.508$	5-50	6-14	18
[19]	$50 \times 74 \times 1$	5-30	4-8	8
Prop	$50 \times 137 \times 0.79$	4-16	8.5-14.5	12

empirical formula in that document [20], and their orientation angle is initially set to 0 degrees. The length of the slit is then measured at 11.2 mm, and the orientation angle is 33° after simulating and optimizing with HFSS V15. By comparing the simulation results, it was found that adding a slot on the outer edge of the radiator did not significantly affect the phase distribution of the antenna aperture.

4. Experimental Results and Discussions

The CAVA and PSEAVA-SPCDL antennas have been designed and tested separately. The photograph of the fabricated antennas with a coaxial connector is shown in Figure 11.

The gain curve of the PSEAVA-SPCDL is shown in Figure 12. It can be observed that the gain of PSEAVA-SPCDL is significantly increased compared to the AVA-SPCDL at 4-8 GHz. In addition, the periodic slit edge technique has little effect on the gain at high frequencies.

The return loss of both fabricated antennas is measured by Agilent Performance Network Analyzer N5224A. We can see that the test's results are in good agreement with the simulation's results. The return loss of the antenna is shown in Figure 13.

Figures 14 and 15 show the *E*-plane and *H*-plane radiation patterns of the CAVA and PSEAVA-PCDL at 4, 8, 12, and 16 GHz. The radiation pattern of the PSEAVA-PCDL has a narrower 3 dB beam width, a lower sidelobe level, and a better directivity performance combined with a higher gain in all frequency bands than the CAVA. The antenna has solved the beam tilt and main lobe-splitting problem in the high frequency, expanding the traditional uses of the Vivaldi antenna application to include situations with higher gain requirements.

5. Conclusion

Based on the phase information of the aperture of the antipodal Vivaldi antenna, an antipodal Vivaldi antenna loaded with a broadband near-field dielectric lens was designed. By applying PSE technology at low frequencies without changing the antenna size, the reflection coefficient and radiation performance can be improved, as shown in Table 3. The return loss of PSEAVA-SPCDL proposed in this paper is less than -10 dB for the entire frequency. The antenna gain is improved from 5.6 dB to 8.6 dB at 4 GHz and from 4.9 dB to 14.5 dB at 16 GHz. Moreover, the tilted beam problem encountered by the CAVA at high frequencies is solved. The directional performance of the proposed antenna has been enhanced, with lower sidelobes in the radiation pattern and a narrower beam width of 3 dB. The antenna is a good choice for high-resolution imaging systems due to its single antenna structure, simple structure, convenient design, and low cost.

Data Availability

The data that support the findings of this study are available from the corresponding author.

Conflicts of Interest

The authors declare that they have no conflicts of interest.

Acknowledgments

This research was funded by the National Key Basic Research Program of China (Grant No. 2019YFA0210204).

References

[1] J. Bourqui, M. Okoniewski, and E. C. Fear, "Balanced antipodal Vivaldi antenna with dielectric director for near-field microwave imaging," *IEEE Transactions on Antennas and Propagation*, vol. 58, no. 7, pp. 2318–2326, 2010.

[2] M. Moosazadeh, S. Kharkovsky, J. T. Case, and B. Samali, "Miniaturized UWB antipodal Vivaldi antenna and its application for detection of void inside concrete specimens," *IEEE Antennas and Wireless Propagation Letters*, vol. 16, pp. 1317–1320, 2017.

[3] "Improved design of the Vivaldi antenna," *IEE Proceedings H Microwaves, Antennas and Propagation*, vol. 135, no. 2, pp. 89–92, 1988.

[4] J. D. S. Langley, P. S. Hall, and P. Newham, "Novel ultrawideband Vivaldi antenna with low crosspolarisation," *Electronics Letters*, vol. 29, no. 23, pp. 2004-2005, 1993.

[5] I. T. Nassar and T. M. Weller, "A novel method for improving antipodal Vivaldi antenna performance," *IEEE Transactions on Antennas and Propagation*, vol. 63, no. 7, pp. 3321–3324, 2015.

[6] M. Moosazadeh and S. Kharkovsky, "A Compact high-gain and front-to-back ratio elliptically tapered antipodal Vivaldi antenna with trapezoid-shaped dielectric lens," *IEEE Antennas and Wireless Propagation Letters*, vol. 15, pp. 552–555, 2016.

[7] H. Liu, W. Yang, A. Zhang, S. Zhu, Z. Wang, and T. Huang, "A miniaturized gain-enhanced antipodal Vivaldi antenna and its array for 5G communication applications," *IEEE Access*, vol. 6, pp. 76282–76288, 2018.

[8] A. M. De Oliveira, M. B. Perotoni, S. T. Kofuji, and J. F. Justo, "A palm tree antipodal Vivaldi antenna with exponential slot edge for improved radiation pattern," *IEEE Antennas and Wireless Propagation Letters*, vol. 14, pp. 1334–1337, 2015.

[9] A. Karmakar, A. Bhattacharjee, A. Saha, and A. Bhawal, "Design of a fractal inspired antipodal Vivaldi antenna with enhanced radiation characteristics for wideband applications," *IET Microwaves, Antennas and Propagation*, vol. 13, no. 7, pp. 892–897, 2019.

[10] M. Moosazadeh and S. Kharkovsky, "Design of ultra-wideband antipodal Vivaldi antenna for microwave imaging applications," in *2015 IEEE International Conference on Ubiquitous Wireless Broadband (ICUWB)*, Montreal, QC, Canada, 2015.

[11] L. Chen, Z. Y. Lei, R. Yang, J. Fan, and X. Shi, "A broadband artificial material for gain enhancement of antipodal tapered slot antenna," *IEEE Transactions on Antennas and Propagation*, vol. 63, no. 1, pp. 395–400, 2015.

[12] M. C. Greenberg, K. L. Virga, and C. L. Hammond, "Performance characteristics of the dual exponentially tapered slot antenna (DETSA) for wireless communications applications," *IEEE Transactions on Vehicular Technology*, vol. 52, no. 2, pp. 305–312, 2003.

[13] B. Zhou, H. Li, X. Y. Zou, and T. J. Cui, "Broadband and high-gain planar vivaldi antennas based on inhomogeneous anisotropic zero-index metamaterials," *Progress In Electromagnetics Research-Pier*, vol. 120, pp. 235–247, 2011.

[14] L. Sang, X. X. Li, T. Chen, and G. Lv, "Analysis and design of tapered slot antenna with high gain for ultra-wideband based on optimisation of the metamaterial unit layout," *IET Microwaves, Antennas and Propagation*, vol. 11, no. 6, pp. 907–914, 2017.

[15] X. X. Li, G. Liu, Y. M. Zhang, L. Sang, and G. Lv, "A compact multi-layer phase correcting lens to improve directive radiation of Vivaldi antenna," *International Journal of RF and Microwave Computer-Aided Engineering*, vol. 27, no. 7, article e21109, 2017.

[16] A. Elsherbini, C. Zhang, S. Lin et al., "UWB antipodal Vivaldi antennas with protruded dielectric rods for higher gain, symmetric patterns and minimal phase center variations," in *2007 IEEE Antennas and Propagation Society International Symposium*, pp. 1973–1976, Honolulu, HI, USA, 2007.

[17] K. Kota and L. Shafai, "Gain and radiation pattern enhancement of balanced antipodal Vivaldi antenna," *Electronics Letters*, vol. 47, no. 5, pp. 303-304, 2011.

[18] A. Molaei, M. Kaboli, S. A. Mirtaheri, and M. S. Abrishamian, "Dielectric lens balanced antipodal Vivaldi antenna with low cross-polarisation for ultra-wideband applications," *IET Microwaves Antennas & Propagation*, vol. 8, no. 14, pp. 1137–1142, 2014.

[19] G. Teni, N. Zhang, J. H. Qiu, and P. Zhang, "Research on a novel miniaturized antipodal Vivaldi antenna with improved radiation," *IEEE Antennas and Wireless Propagation Letters*, vol. 12, pp. 417–420, 2013.

[20] M. Amiri, F. Tofigh, A. Ghafoorzadeh-Yazdi, and M. Abolhasan, "Exponential antipodal Vivaldi antenna with exponential dielectric lens," *IEEE Antennas and Wireless Propagation Letters*, vol. 16, pp. 1792–1795, 2017.

[21] M. Moosazadeh, S. Kharkovsky, and J. T. Case, "Microwave and millimetre wave antipodal Vivaldi antenna with trapezoid-shaped dielectric lens for imaging of construction materials," *IET Microwaves, Antennas and Propagation*, vol. 10, no. 3, pp. 301–309, 2016.

[22] M. Moosazadeh, S. Kharkovsky, J. T. Case, and B. Samali, "Improved radiation characteristics of small antipodal Vivaldi antenna for microwave and millimeter-wave imaging applications," *IEEE Antennas and Wireless Propagation Letters*, vol. 16, pp. 1961–1964, 2017.